

Dynamic range of atomically thin vibrating nanomechanical resonators

Zenghui Wang and Philip X.-L. Feng^{a)}

Department of Electrical Engineering and Computer Science, Case School of Engineering, Case Western Reserve University, 10900 Euclid Avenue, Cleveland, Ohio 44106, USA

(Received 16 January 2014; accepted 24 February 2014; published online 12 March 2014)

Atomically thin two-dimensional (2D) crystals offer attractive properties for making resonant nanoelectromechanical systems (NEMS) operating at high frequencies. While the fundamental limits of linear operation in such systems are important, currently there is very little quantitative knowledge of the linear dynamic range (DR) and onset of nonlinearity in these devices, which are different than in conventional 1D NEMS such as nanotubes and nanowires. Here, we present theoretical analysis and quantitative models that can be directly used to predict the DR of vibrating 2D circular drumhead NEMS resonators. We show that DR has a strong dependence $\propto 10 \log(E_Y^{5/2} \rho_{3D}^{-1/2} r t \epsilon^{5/2})$ on device parameters, in which strain ϵ plays a particularly important role in these 2D systems, dominating over dimensions (radius r , thickness t). This study formulizes the effects from device physical parameters upon DR and sheds light on device design rules toward achieving high DR in 2D NEMS vibrating at radio and microwave frequencies. © 2014 AIP Publishing LLC.
[\[http://dx.doi.org/10.1063/1.4868129\]](http://dx.doi.org/10.1063/1.4868129)

Nanoelectromechanical systems (NEMS) have enabled interesting fundamental studies and technological applications by coupling mechanical degrees of freedom with other physical properties in structures at scales approaching the fundamental limit.¹ Two-dimensional (2D) nanomaterials^{2–4} are attractive for making NEMS because they offer extremely light weight, ultrahigh mechanical flexibility, exceptionally high mechanical strength, and robust nanomechanical resonances, in addition to other interesting physical and chemical properties in atomically-thin membranes. This combination of unique device geometry (miniature size and very high aspect ratio, size/thickness) and compelling material properties makes 2D NEMS interesting for both fundamental device studies and potential applications, such as charge density wave detection,⁵ surface adsorption sensing,⁶ and signal processing.⁷ For all these applications, one important aspect in device performance is the dynamic range (DR), the ratio between the highest signal level prior to any nonlinear bifurcation (“signal ceiling”) and the lowest detectable level (“noise floor”). This allowable range of signal-to-noise ratio (often in decibels, dB) sets the linear operating range of the device as a transducer. The signal ceiling is determined by the onset of nonlinearity,^{8,9} and the noise floor is set by all noise processes in measuring device motion.^{10,11}

As continued miniaturization of resonant NEMS advances from conventional thin film structures into atomically thin 2D NEMS, devices become increasingly susceptible to external stimuli (thus increasing responsivity), while noise may also increase due to thermal fluctuations (inversely proportional to device mass) and thus could limit the linear operation. To date, in very few experimental studies DR values (in dB) have been estimated for 2D NEMS,^{6,12,13} but neither direct measurement of DR nor its analytical model has been reported, lacking a systematic investigation. Although analysis of beam-structured 1D NEMS resonators suggests

that devices with smaller cross-sectional areas have lower DR (e.g., few-micron long single-walled carbon nanotube’s DR is expected to fall below 0 dB, thus completely incompetent as a linear transducer),¹¹ how to quantitatively estimate DR of 2D NEMS is unknown, and the scaling laws and conclusions in previous 1D devices are not simply applicable to 2D NEMS.

In this Letter, we present a detailed theoretical analysis of how the intrinsic DR of these 2D NEMS resonators depends on various devices parameters—including size, number of layers (i.e., discrete thickness), and initial built-in tension. In addition, because these ultimately thin 2D NEMS devices also make an attractive platform for “putting mechanics into quantum mechanics,”^{14–17} we investigate the device motions near their quantum limit at low temperatures and show how quantum phenomena affect the device linear dynamic range.

While 1D NEMS resonators may be modeled as strings, beams, or hanging chains,¹⁸ 2D devices with thickness of only one to few atomic layers behave universally as membranes in the presence of nonzero tension⁴ due to their much lower and even negligible bending rigidities in this regime.^{19–21} While doubly-clamped structures with open sides and edges have been investigated,^{6,12,22–27} the coexistence of clamped and free boundaries, and defects along the edges, could cause stress localization and excess dissipation processes.²⁸ Fully clamped structures such as square or circular membranes possess well-defined boundary conditions and exhibit predictable resonance behavior.^{4,13,29,30} As illustrated in Fig. 1(a), here we focus on modeling fully clamped circular membranes under tension to examine the DR of these 2D NEMS resonators.

We consider nanomechanical nonlinearity in the resonant motion of a circular membrane arising from the deflection-induced tension.^{31,32} The equation of motion is⁸

$$\ddot{x} + \frac{\omega_0}{Q} \dot{x} + \omega_0^2 x + \omega_0^2 \kappa^2 x^3 = \frac{F_{ext}}{M_{eff}}, \quad (1)$$

with ω_0 , Q , F_{ext} , and M_{eff} being the angular resonance frequency, quality factor, external drive force, and effective

^{a)} Author to whom correspondence should be addressed. Electronic mail: philip.feng@case.edu

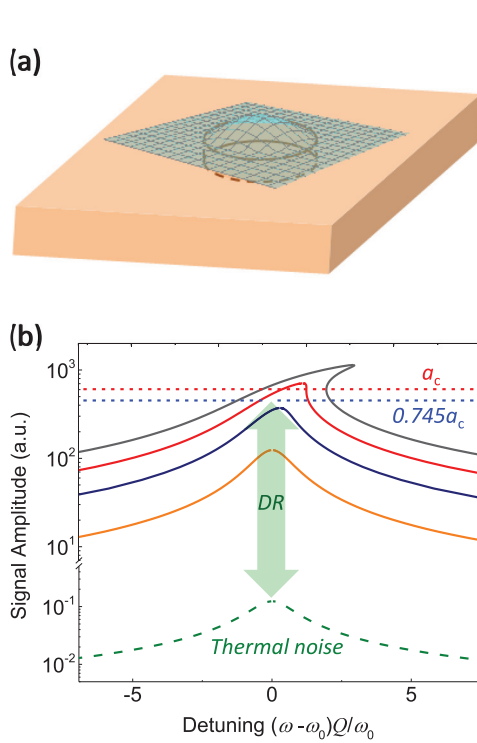


FIG. 1. (a) Schematic of a 2D circular membrane NEMS resonator, with illustration of the mode shape of the fundamental resonance mode. (b) Nonlinear response of a Duffing resonator. Bottom dashed curve: Thermomechanical noise. Solid lines: Frequency response curves under different driving amplitudes. Dotted lines: The critical amplitude a_c and the 1 dB compression point $0.745a_c$. Double-ended arrow: Dynamic range for linear operation.

modal mass, respectively. The Duffing-type nonlinear coefficient κ for circular membrane is³²

$$\kappa^2 = \frac{13 + 21\nu - 4\nu^2}{30(1 + \nu)r^2\varepsilon}, \quad (2)$$

where ν is Poisson's ratio of the material, r is the membrane radius, and ε is the initial strain. The critical amplitude a_c , which determines the onset of bistability, is given by

$$a_c = \sqrt{\frac{8\sqrt{3}}{9\kappa^2 Q}}, \quad (3)$$

for circular membranes. Illustration of driven responses of a Duffing resonator is shown in Fig. 1(b), with the critical amplitude highlighted. A conventional measure for the upper limit of the linear operating range is $0.745a_c$, the 1 dB compression point below a_c .¹¹

The lower limit, i.e., the noise floor, is intrinsically limited by the Brownian motion of the device, which has a displacement-domain spectral density

$$S_{x,th}^{1/2}(\omega_0) = \sqrt{\frac{4k_B T Q}{\omega_0^3 M_{eff}}}, \quad (4)$$

where k_B is Boltzmann constant and T is temperature.

The dynamic range for linear operation is then defined by the ratio (in dB) between the 1 dB compression point and the noise floor¹¹

$$DR \equiv 20 \log \left(\frac{0.745a_c}{\sqrt{2S_{x,th}\Delta f}} \right), \quad (5)$$

where Δf is the measurement bandwidth (we follow the $\Delta f = 1$ Hz convention in all numerical calculations). Using $\omega_0 = \frac{2.405}{r} \sqrt{\frac{\varepsilon E_Y t}{\rho_{3D}}}$ and $M_{eff} = 0.2695 \rho_{3D} \pi r^2 t$ for circular membranes (E_Y : Young's modulus; t : thickness; ρ_{3D} : 3D mass density of the material), from Eqs. (2) to (5), we obtain

$$DR = const. + 10 \log \left(\frac{1}{\Delta f} \frac{1 + \nu}{13 + 21\nu - 4\nu^2} \frac{1}{k_B T Q^2} \right) + 10 \log \left(\frac{rt\varepsilon^{5/2} E_Y^{3/2}}{\rho_{3D}^{1/2}} \right). \quad (6)$$

We note that the Q s of devices can be affected by many factors (e.g., temperature, pressure, and viscosity of surrounding medium, etc.)—for example, often Q s can increase by

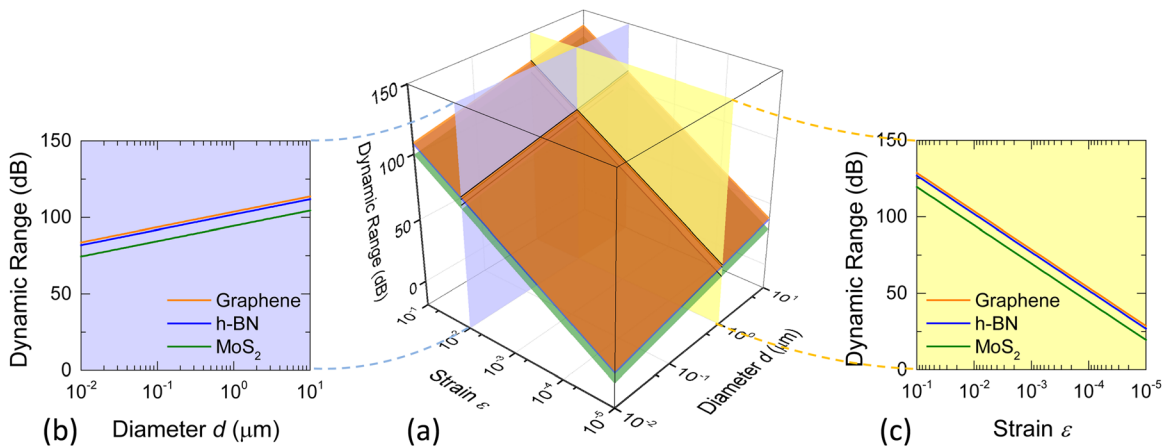


FIG. 2. Intrinsic dynamic range of 2D NEMS resonators at 300 K. (a) DR of single layer graphene, h-BN, and MoS₂ circular drumhead resonators of various diameters (10 nm—10 μ m) and under different strain levels (10 ppm—10%). Purple and yellow intercepting planes represent strain $\varepsilon = 0.01$ (1%) and diameter $d = 1 \mu$ m surfaces in the 3D parameter space. (b) 2D cross-section plot (DR as a function of d) of the $\varepsilon = 0.01$ plane. (c) 2D cross-section plot (DR as a function of ε) of the $d = 1 \mu$ m plane. We use the following parameters in calculation: MoS₂: $t = 0.7$ nm, $E_Y = 0.2$ TPa, $\nu = 0.25$, $\rho_{3D} = 5060$ kg/m³; BN: $t = 0.33$ nm, $E_Y = 0.75$ TPa, $\nu = 0.167$, $\rho_{3D} = 2100$ kg/m³; graphene: $t = 0.34$ nm, $E_Y = 1$ TPa, $\nu = 0.165$, $\rho_{3D} = 2200$ kg/m³.

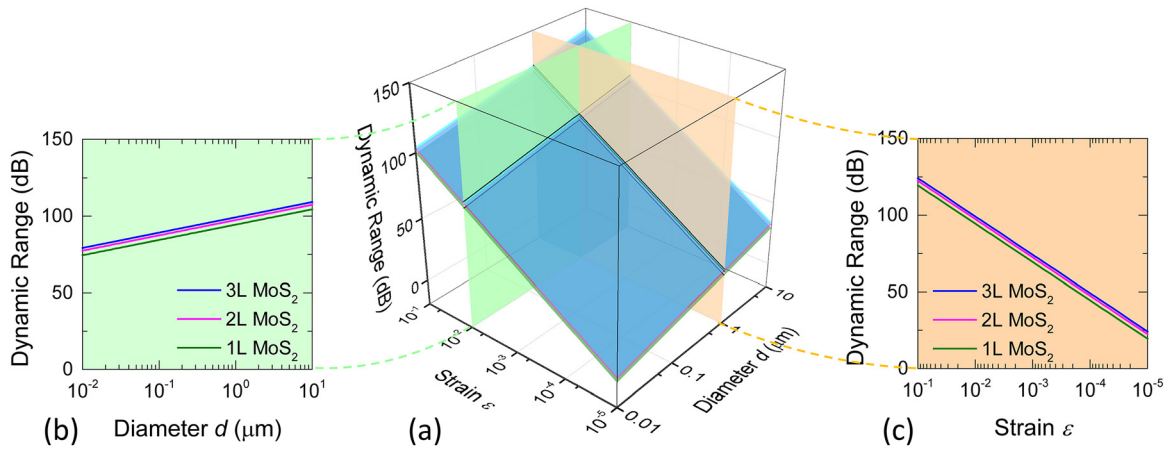


FIG. 3. Intrinsic dynamic range of MoS₂ NEMS resonators of different layer numbers at 300 K. (a) DR of 1, 2, and 3 layer MoS₂ circular drumhead resonators of various diameters (10 nm—10 μm) and under different strain levels (10 ppm—10%). Green and orange intercepting planes represent strain $\varepsilon = 0.01$ (1%) and diameter $d = 1 \mu\text{m}$ surfaces in the 3D parameter space. (b) 2D cross-section plot (DR as a function of d) of the $\varepsilon = 0.01$ plane. (c) 2D cross-section plot (DR as a function of ε) of the $d = 1 \mu\text{m}$ plane.

cooling the devices from room temperature^{6,12,23,25,28} to cryogenic temperatures in ultrahigh vacuum.^{6,23,25,27} For simplicity of numerical computation employing our model, as a reasonable estimate for 2D resonators operating in vacuum, we use an intermediate value of $Q = 1000$ throughout our numerical calculations.

Figure 2 depicts the intrinsic dynamic ranges of monolayer graphene, molybdenum disulfide (MoS₂), and hexagonal boron nitride (h-BN) circular membrane resonators of various diameters and initial tension values (we use diameter $d = 2r$ in the plots) at room temperature (300 K). From the plots, we can see that the dynamic range for 2D NEMS resonators increases with device diameter, in contrast to the 1D case where DR decreases with device length. This difference exemplifies the effect of dimensionality on scaling laws. In the 1D case, frequency scales with device length L as $\omega_0 \sim L^{-2}$, while approximately $a_c \sim L$ for large L values under nonzero tension,¹¹ and $M_{\text{eff}} \sim L$. As a result, $\text{DR} \sim 20 \log(L^{-3/2})$. In 2D membranes, $\omega_0 \sim d^{-1}$, $M_{\text{eff}} \sim d^2$, and $a_c \sim d$, thus $\text{DR} \sim 20 \log(d^{1/2})$. Therefore, opposed to their 1D counterparts, 2D NEMS devices can benefit from larger aspect ratios (lateral dimension *versus* thickness, e.g., r/t or d/t), which lead to greater DR. Importantly, the effect from tension/strain is more pronounced than that from device dimensions. From Eqs. (2) and (3), one has $a_c \sim \varepsilon^{1/2}$, and with $\omega \sim \varepsilon^{1/2}$, it yields $\text{DR} \sim 20 \log(\varepsilon^{5/4})$, as clearly shown in Fig. 2(c) (note the polarity of the horizontal axis). This suggests that, together with the ultrahigh strain limit in these 2D membranes (often up to $\sim 10\%$ to 20% , orders of magnitude higher than in conventional structures), device strain can be harnessed as a highly effective tuning mechanism for engineering the device dynamic range.

One feature inherent to NEMS resonators based on 2D layered materials is the discreteness in device thickness, which sets a fundamental distinction between these atomically-thin layers and macroscale membranes. From Eq. (6), we expect that for the same material (given E_Y and ρ_{3D}), devices with fewer layers (smaller t) exhibit smaller DR. Figure 3 plots the intrinsic DR for 1-, 2-, and 3-layer MoS₂ circular drumhead resonators. Thinner devices clearly show

lower dynamic range (with other device parameters given), due to the higher thermal noise motion amplitude arising from their smaller motional masses. This discretization of DR with number of layers is an intriguing signature of layered 2D materials and should be exploited in future device applications. For example, linear resonators may be employed for radio frequency (RF) signal processing,³³ and nonlinear resonators can be harnessed to create logic and memory building blocks.³⁴ Under a given drive, using a universal tension tuning mechanism (e.g., a back gate), it may be possible to selectively set all the 1-layer (1L) devices into the nonlinear regime, while the 2L and 3L devices remain linear. This controlled selectivity can be used to build reconfigurable mechanical circuits from these 2D materials, where devices with different layer numbers can be selectively toggled between different functions in a programmable way.

We now examine the DR of 2D devices at cryogenic temperatures, where quantum effects become dominant. NEMS devices operating near or at the quantum limit are of considerable interest for both fundamental physics and quantum information processing applications.^{14–17,35–41} The dynamic range of their quantum mechanical motion determines the usefulness of these devices as linear sensors for quantum-limit

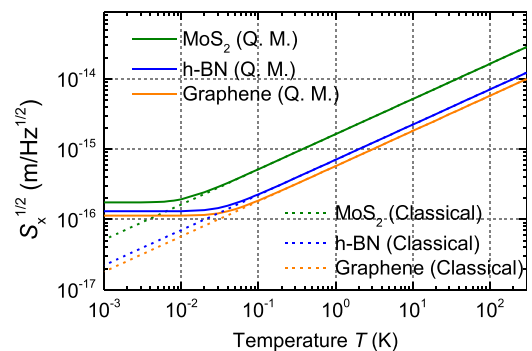


FIG. 4. Thermomechanical noise spectral density as a function of temperature for 2D NEMS resonators (single layer graphene, h-BN, and MoS₂) with strain $\varepsilon = 0.01$ (1%) and diameter $d = 1 \mu\text{m}$. Dashed lines show results from equipartition theorem (Eq. (4)), and solid lines are calculated with quantum fluctuation-dissipation theorem (Eq. (7)).

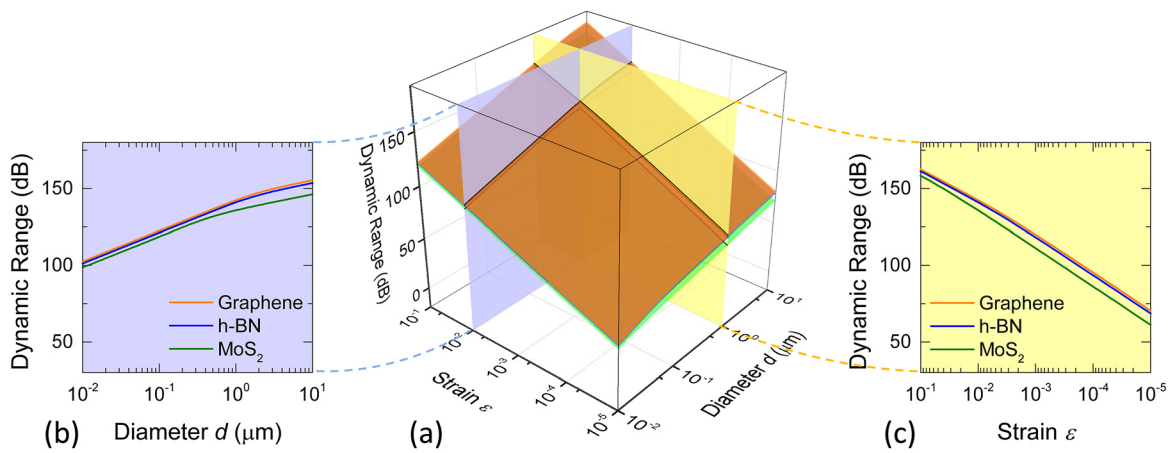


FIG. 5. Intrinsic dynamic range of 2D NEMS resonators at 20 mK. (a) DR of single layer graphene, h-BN, and MoS₂ circular drumhead resonators of various diameters (10 nm—10 μm) and under different strain levels (10 ppm—10%). Purple and yellow intercepting planes represent strain $\varepsilon = 0.01$ (1%) and diameter $d = 1 \mu\text{m}$ surfaces in the 3D parameter space. (b) 2D cross-section plot (DR as a function of d) of the $\varepsilon = 0.01$ plane. (c) 2D cross-section plot (DR as a function of ε) of the $d = 1 \mu\text{m}$ plane.

applications such as gravitational wave detection⁴² and single molecule MRI.⁴³ As the device temperature continues to decrease, thermomechanical motions (spectral density given in Eq. (4)) gradually give way to quantum fluctuations as the ratio $\hbar\omega_0/k_B T$ continues to increase. By substituting the thermal energy $k_B T$ with the thermally averaged quantum energy (with zero-point energy taken into account),⁴⁴ the quantum mechanical motion spectral density is⁴⁵

$$S_{x,QM}^{1/2}(\omega_0) = \sqrt{2\hbar\omega_0 \coth\left(\frac{\hbar\omega_0}{2k_B T}\right) \frac{Q}{\omega_0^3 M_{eff}}}, \quad (7)$$

which, in the high temperature limit of $k_B T \gg \hbar\omega_0$, degenerates to Eq. (4). Figure 4 displays $S_x^{1/2}$ as a function of temperature for single-layer graphene, h-BN, and MoS₂ devices with $d = 1 \mu\text{m}$ and $\varepsilon = 0.01$ (1%). The deviation from classical statistical mechanics is evident below 100 mK, with different onset temperatures for different 2D NEMS. Below 10 mK the decreasing trend of $S_x^{1/2}$ ceases, with the values asymptotically approaching the quantum zero-point energy.

By substituting Eq. (4) with the expression given by the quantum fluctuation-dissipation theorem (Eq. (7)), we calculate the quantum-limited DR for 2D resonators using Eq. (5) and plot the results in Fig. 5. Significant quantum effect is found at low temperatures, which reduces the DR for linear operation. In Fig. 5(b), the right side of the curves (larger diameter) has the same slope as in Fig. 2(b), as bigger devices have stronger tendency to remain classical. As device size decreases (left side of the plot), the resonance frequency increases and quantum effects become more pronounced. Once quantum fluctuations replace thermomechanical motions and become the noise floor (Fig. 4, left end), the DR is further reduced from the classical case and the curves (in Fig. 5(b)) assume a steeper slope. Note the sequence of different devices entering the quantum regime is similar to that in Fig. 4. Similarly, in Fig. 5(c), the right side represents the classical regime with slope of the curves identical to that in Fig. 2(c), and the left side shows the quantum effect, as greater strain increases the resonance frequency which allows the quantum effect to be better observed.

To experimentally verify the predictions of DR with our theoretical model (Eq. (6)), one needs to precisely measure both the intrinsic thermomechanical noise and the onset of mechanical nonlinearity in the same 2D resonator. In recent experiments, either of these has been measured separately,^{4,6,12,13} but not yet both, due to practical limitations in the detection and actuation techniques employed. We anticipate that advances in experimental schemes can lead to accurate measurement of DR in devices with various dimensions and tension levels, to validate the DR prediction and its scaling law.

In summary, we have shown that 2D NEMS resonators are intrinsically different than their 1D counterparts in terms of scaling laws for dynamic range, with dependence $\propto 10 \log[r t \varepsilon^{5/2}]$. Larger 2D devices have greater DR due to reduced thermal fluctuations and deferred onset of bistability. Device initial strain (ε) has stronger effects on the dynamic range than the dimensional parameters (r , t) do and should be exploited for its efficient DR tuning mechanism. These findings suggest that 2D NEMS devices (in contrast to 1D ones) are particularly suited for DR-sensitive applications, and can offer broader and highly tunable dynamic ranges.

This work was supported by Case School of Engineering, a T. Keith Glennan Fellowship, and an ACES+ Advance Opportunity Award.

¹M. L. Roukes, *Scientific American* **285**, 48 (2001).

²R. A. Barton, J. Parpia, and H. G. Craighead, *J. Vac. Sci. Technol. B* **29**, 050801 (2011).

³Z. Wang, J. Lee, K. He, J. Shan, and P. X.-L. Feng, *Sci. Rep.* **4**, 3919 (2014).

⁴J. Lee, Z. Wang, K. He, J. Shan, and P. X.-L. Feng, *ACS Nano* **7**, 6086 (2013).

⁵S. Sengupta, H. S. Solanki, V. Singh, S. Dhara, and M. M. Deshmukh, *Phys. Rev. B* **82**, 155432 (2010).

⁶C. Chen, S. Rosenblatt, K. I. Bolotin, W. Kalb, P. Kim, I. Kymissis, H. L. Stormer, T. F. Heinz, and J. Hone, *Nat. Nanotechnol.* **4**, 861 (2009).

⁷C. Chen, S. Lee, V. V. Deshpande, G.-H. Lee, M. Lekas, K. Shepard, and J. Hone, *Nat. Nanotechnol.* **8**, 923 (2013).

⁸A. H. Nayfeh and D. T. Mook, *Nonlinear Oscillations* (John Wiley, New York, 1979).

⁹I. Kozinsky, H. W. C. Postma, I. Bargatin, and M. L. Roukes, *Appl. Phys. Lett.* **88**, 253101 (2006).

- ¹⁰A. N. Cleland, *Foundations of Nanomechanics* (Springer-Verlag, New York, 2003).
- ¹¹H. W. Postma, I. Kozinsky, A. Husain, and M. L. Roukes, *Appl. Phys. Lett.* **86**, 223105 (2005).
- ¹²J. S. Bunch, A. M. van der Zande, S. S. Verbridge, I. M. Frank, D. M. Tanenbaum, J. M. Parpia, H. G. Craighead, and P. L. McEuen, *Science* **315**, 490 (2007).
- ¹³R. A. Barton, B. Ilic, A. M. van der Zande, W. S. Whitney, P. L. McEuen, J. M. Parpia, and H. G. Craighead, *Nano Lett.* **11**, 1232 (2011).
- ¹⁴K. Schwab and M. L. Roukes, *Phys. Today* **58**(7), 36 (2005).
- ¹⁵A. D. O'Connell, M. Hofheinz, M. Ansmann, R. C. Bialczak, M. Lenander, E. Lucero, M. Neeley, D. Sank, H. Wang, M. Weides *et al.*, *Nature* **464**, 697 (2010).
- ¹⁶J. D. Teufel, T. Donner, D. Li, J. W. Harlow, M. S. Allman, K. Cicak, A. J. Sirois, J. D. Whittaker, K. W. Lehnert, and R. W. Simmonds, *Nature* **475**, 359 (2011).
- ¹⁷J. Chan, T. P. M. Alegre, A. H. Safavi-Naeini, J. T. Hill, A. Krause, S. Gröblacher, M. Aspelmeyer, and O. Painter, *Nature* **478**, 89 (2011).
- ¹⁸V. Sazonova, Y. Yaish, H. Ustunel, D. Roundy, T. A. Arias, and P. L. McEuen, *Nature* **431**, 284 (2004).
- ¹⁹Y. Wei, B. Wang, J. Wu, R. Yang, and M. L. Dunn, *Nano Lett.* **13**, 26 (2013).
- ²⁰N. Lindahl, D. Midtvedt, J. Svensson, O. A. Nerushev, N. Lindval, A. Isacsson, and E. E. B. Campbell, *Nano Lett.* **12**, 3526 (2012).
- ²¹J.-W. Jiang, Z. Qi, H. S. Park, and T. Rabczuk, *Nanotechnology* **24**, 435705 (2013).
- ²²X. Song, M. Oksanen, M. A. Sillanpää, H. G. Craighead, J. M. Parpia, and P. J. Hakonen, *Nano Lett.* **12**, 198 (2012).
- ²³V. Singh, S. Sengupta, H. S. Solanki, R. Dhall, A. Allain, S. Dhara, P. Pant, and M. M. Deshmukh, *Nanotechnology* **21**, 165204 (2010).
- ²⁴Y. Xu, C. Chen, V. V. Deshpande, F. A. DiRenno, A. Gondarenko, D. B. Heinz, S. Liu, P. Kim, and J. Hone, *Appl. Phys. Lett.* **97**, 243111 (2010).
- ²⁵A. M. van der Zande, R. A. Barton, J. S. Alden, C. S. Ruiz-Vargas, W. S. Whitney, P. H. Q. Pham, J. W. Park, J. M. Parpia, H. G. Craighead, and P. L. McEuen, *Nano Lett.* **10**, 4869 (2010).
- ²⁶Y. Oshidari, T. Hatakeyama, R. Kometani, S. Warisawa, and S. Ishihara, *Appl. Phys. Express* **5**, 117201 (2012).
- ²⁷A. Eichler, J. Moser, J. Chaste, M. Zdrojek, I. Wilson-Rae, and A. Bachtold, *Nat. Nanotechnol.* **6**, 339 (2011).
- ²⁸D. Garcia-Sanchez, A. M. van der Zande, A. San Paulo, B. Lassagne, P. L. McEuen, and A. Bachtold, *Nano Lett.* **8**, 1399 (2008).
- ²⁹S. Lee, C. Chen, V. V. Deshpande, G.-H. Lee, I. Lee, M. Lekas, A. Gondarenko, Y.-J. Yu, K. Shepard, P. Kim *et al.*, *Appl. Phys. Lett.* **102**, 153101 (2013).
- ³⁰R. A. Barton, I. R. Storch, V. P. Adiga, R. Sakakibara, B. R. Cipriany, B. Ilic, S. P. Wang, P. Ong, P. L. McEuen, J. M. Parpia, and H. G. Craighead, *Nano Lett.* **12**, 4681 (2012).
- ³¹A. M. Eriksson, D. Midtvedt, A. Croy, and A. Isacsson, *Nanotechnology* **24**, 395702 (2013).
- ³²V. A. Chobotov and R. C. Binder, *J. Acoust. Soc. Am.* **36**, 59 (1964).
- ³³C. T.-C. Nguyen, *IEEE Trans. Ultrason. Ferroelectr. Freq. Control* **54**, 251 (2007).
- ³⁴I. Mahboob and H. Yamaguchi, *Nat. Nanotechnol.* **3**, 275 (2008).
- ³⁵M. D. LaHaye, O. Buu, B. Camarota, and K. C. Schwab, *Science* **304**, 74 (2004).
- ³⁶S. Gigan, H. R. Bohm, M. Paternostro, F. Blaser, G. Langer, J. B. Hertzberg, K. C. Schwab, D. Bauerle, M. Aspelmeyer, and A. Zeilinger, *Nature* **444**, 67 (2006).
- ³⁷C. A. Regal, J. D. Teufel, and K. W. Lehnert, *Nat. Phys.* **4**, 555 (2008).
- ³⁸Y.-S. Park and H. Wang, *Nat. Phys.* **5**, 489 (2009).
- ³⁹S. Gröblacher, J. B. Hertzberg, M. R. Vanner, G. D. Cole, S. Gigan, K. C. Schwab, and M. Aspelmeyer, *Nat. Phys.* **5**, 485 (2009).
- ⁴⁰A. Schliesser, O. Arcizet, R. Rivière, G. Anetsberger, and T. J. Kippenberg, *Nat. Phys.* **5**, 509 (2009).
- ⁴¹T. Rocheleau, T. Ndukum, C. Macklin, J. B. Hertzberg, A. A. Clerk, and K. C. Schwab, *Nature* **463**, 72 (2010).
- ⁴²M. E. Tobar and D. G. Blair, *Rev. Sci. Instrum.* **66**, 2751 (1995).
- ⁴³J. A. Sidles, J. L. Garbini, K. J. Bruland, D. Rugar, O. Züger, S. Hoen, and C. S. Yannoni, *Rev. Mod. Phys.* **67**, 249 (1995).
- ⁴⁴H. B. Callen and T. A. Welton, *Phys. Rev.* **83**, 34 (1951).
- ⁴⁵C. Stampfer, S. Rotter, and J. Burgdörfer, *Appl. Phys. Lett.* **88**, 036101 (2006).